DIFFUSION OF LOW ENERGY AURORAL ELECTRONS IN THE ATMOSPHERE

JUNE 1964

GODDARD SPACE FLIGHT CENTER
GREENBELT, MARYLAND

DIFFUSION OF LOW ENERGY AURORAL ELECTRONS
IN THE ATMOSPHERE

by

Kaichi Maeda

NASA—Goddard Space Flight Center
Greenbelt, Maryland

ABSTRACT

By means of the Monte Carlo method, Spencer's work on the energy dissipation of electrons in air is extended below 25 Kev, and the results are applied to the diffusion of mono-energetic electrons in the polar atmosphere. The results show significant effects of straggling, not only on the distribution of the most penetrating flux but also on the height of maximum dissipation and on the back-scattering. The dependence of back-scattering on the angular distributions as well as the energies of incident electrons are calculated, indicating that it decreases rapidly below 10 Kev and that a maximum of back-scattering seems to occur at energies around 20 Kev, with values of the order of 7% and 20% for vertical and isotropic incidence, respectively for intensity. Corresponding energy back-scattering coefficients (albedos) are approximately half of these values.

i

DIFFUSION OF LOW ENERGY AURORAL ELECTRONS
IN THE ATMOSPHERE

1. Introduction

In calculating the rates of reactions caused by auroral activities
(such as the vertical distributions of luminosity and auroral absorption
or the rate of dissociation of air due to bombarding auroral particles) it
is necessary to have fundamental information on the behavior of primary
auroral particles in the upper atmosphere. This information includes
changes of intensity (particle flux) and of energy flux, and the rate of
these changes with atmospheric depth.

Actually these can be calculated easily with the required accuracy
by using range-energy relations for protons but not for electrons. (Rossi,
1952; Maeda and Singer, 1961; Maeda, 1962, 1963 a,b). Because of the
dominating effect of Coulomb scattering and its statistical nature in
collision processes, no rigorous calculations are available for these
purposes, except for an extensive computation on the energy dissipation
of electrons done by V. L. Spencer (1959).

Recently, M. H. Rees (1963) made semi-empirical calculations on
the luminosity distribution of aurora, which are based on the laboratory
data given by A. E. Grün (1957). Since Grün's measurements are limited
in the case of the vertical incidence of mono-energetic electrons with
energies between 5 and 54 Kev, Rees had to make some ad hoc assump-
tions on angular distribution in order to extend Grün's results to other cases.

The purpose of the present calculations is, therefore, as follows:

(1) To extend Spencer's work below 25 Kev, because most auroral electrons are in this energy range.

(2) To find not only the energy dissipation rates in air and the amount of back-scattering but also the changes of angular distributions and of energy spectra with depth due to scattering and straggling.

(3) To apply the results to the diffusion of mono-energetic auroral electrons in the atmosphere.

The importance of the straggling effect on penetrating electrons has been mentioned in several papers concerning the tail part of intensity and of the energy distribution of electrons (Spencer, 1959; Grün, 1957; Perkins, 1962; Rees, 1963). These tailing distributions are due to both scattering and fluctuation in the energy loss rate at each collision. Therefore, sometimes the word "straggling" is used for those combined effects. In this paper, however, the straggling effect means only the effect due to fluctuations in energy loss, namely, the effect due only to Landau fluctuation (1944).

It should be noted that Spencer's calculation, which is based on the so-called moments method, cannot take the straggling effect into account. At present the only way to take these effects, as well as multiple Coulomb scattering and continuous energy loss, into consideration simultaneously is by the Monte Carlo method.

Since the geomagnetic field is nearly vertical and uniform in the polar region, the unwinding of the spiraling path of impinging electrons

is equivalent to the oblique path with the incident angle equal to the pitch angle. Therefore, the results of computations which are performed with respect to the air, assuming uniform density without a magnetic field, are applied to the electrons diffusing into the polar upper atmosphere by using the CIRA atmospheric model (Kallmann-Bijl, et al, 1961).

2. Calculations

The Monte Carlo calculation consists essentially of two parts, namely, the basic data which contain formulas for scattering and energy loss as a function of the energy of electrons in the medium (i.e., in air), and the random sampling for combinations of these basic data for a given number of histories.

The programs for machine calculation have been made at several places for different purposes. A review on this type of calculation is given by M. J. Berger (1963). Details of the program (Fortran for IBM 7090) used in the present calculation have been published by Berger (1963). Similar reports also have been written recently by Berger and Seltzer (1964 a, b).

The formulas used for the basic data are as follows:

(1) Energy loss. Since the energies of electrons in the present calculation are below 25 Kev, radiation losses are completely neglected. Electron trajectories are schematically divided into a number of short sections, whose lengths are chosen so that a mean energy loss in each section corresponds to a certain factor ($2^{-1/16}$ in most cases) of

3

reduction of the electron energy. The mean energy loss is calculated according to the Bethe theory formulated by Rohrlich and Carlson (1954).

(2) Angular deflection. For the angular distribution, the multiple scattering theory of Goudsmit and Saunderson (1940) with Mott's cross section for single scattering (Mott, 1929) is used instead of the familiar Moliere's theory for multiple Coulomb scattering (Moliere, 1948). This gives better accuracy for a large deflection.

(3) Straggling. The expression for fluctuation of the energy loss from a continuous loss rate is taken from the paper by Blunck and Leisegang (1950) instead of using the original expression by Landau (1944).

The basic quantity to be computed is

$$T(E_0, \cos \theta_0 \ E, \cos \theta, x) \ dE \cdot d \cos \theta. \qquad (1)$$

This is called the differential transmission (Berger, 1963). It represents the probability that an electron with initial energy E_0 at an incident angle θ_0 from the normal direction will appear at a depth x energy with E at an angle θ (between $\cos \theta$ and $\cos \theta + d \cos \theta$). The depth x is expressed by the units of range r_0, i.e., $x = r/r_0$ where r is the thickness of the layer in g/cm^2 and r_0 is

$$r_0 = \int_0^{E_0} dE \left/ \left(- \frac{dE}{dx} \right) \right. \qquad (2)$$

4

The Bethe formula is used for $-dE/dx$. Range r_0 in g cm^{-2} and height Z_0 in CIRA (1961) model corresponding r_0 for given E_0 are shown in Table 1.

The other quantities of interest are obtained by summing the differential transmission as follows:

(1)   The relative energy spectrum at x is

$$i\,(E_0,\ E,\ x) = \int_0^1 T\,(E_0,\ E,\ \cos\theta,\ x)\ d\cos\theta \qquad (3)$$

(2)   The relative intensity is

$$\frac{I\,(E_0,\ x)}{I_0} = \int_{E_c}^{E_0} i\,(E_0,\ E,\ x)\ dE \qquad (4)$$

(3)   The relative energy flux is

$$\frac{E(x)}{E_0} = \frac{1}{E_0} \int_0^1 d\cos\theta \int_{E_c}^{E_0} E\cdot T\,(E_0,\ E,\ x,\ \cos\theta)\ dE \qquad (5)$$

(4)   The integrated relative angular distribution is

$$j\,(E_0,\ x,\ \cos\theta) = \int_{E_c}^{E_0} T\,(E_0,\ E,\ x,\ \cos\theta)\ d\cos\theta \qquad (6)$$

The isotropic incident case is given by integrating the initial distribution with respect to $d\cos\theta_0$ with a weight function $\cos\theta_0$.

5

Normalization of the above quantities corresponds to using 10,000 incident electrons in the calculations; i.e.,

$$I_0 = \int_{E_i}^{E_0} i(E_0, E, 0) \, dE = 10^4, \text{ and}$$

E_c is taken as 10^{-3}. E_0 for all cases.

3. Results

Except for the angular dependence of back-scattering, the following results are based on the analysis of 2,000 Monte Carlo histories, with two cases of incident angular distribution (i.e., vertical and isotropic distribution), for initial energies of 20, 10, 5, and 2.5 Kev. To show the effect of straggling, all calculations are done in two ways—one includes straggling and the other does not.

3.1 Relative intensity, $I(x)/I_0$

The relative intensity is shown in Fig. 1 (a-b) for $E_0 = 20$ and 2.5 Kev against depth x . Full and dashed lines stand for the cases with straggling and without straggling, respectively. It should be noted that longer tails of intensity distribution due to straggling effects have been shown by several laboratory experiments (Grün, 1957, Frank, 1959) for vertical incidence.

3.2 Energy flux $E(x)/E_0$

Corresponding to Fig. 1 (a-b), the energy flux is shown in Fig. 2 (a-b) for $E_0 = 20$ and 2.5 Kev against x. Full and dashed lines stand for the cases with straggling and without straggling, respectively.

3.3 Relative Energy Dissipation $\frac{1}{E_0} \cdot \frac{dE}{dx}$

By differentiating the energy flux curve with respect to depth x, relative energy dissipation can be obtained as shown in Fig. 3 (a-b). From this we can see that the form of the energy dissipation curve changes with energy below 20 Kev. Therefore, the conventional assumption of relative dissipation curves independent of energies is incorrect below 25 Kev.

3.4 Angular dependence of back-scattering

The ratio of back-scattered intensity (or energy flux) to incident intensity (or incident energy flux), is called the back-scattering coefficient or back diffusion coefficient (Frank, 1959; Wu, 1960). Experimentally, it is known that this coefficient is quite large for large Z material (approximately 50% for P b, $Z = 82$) but it is regarded as neglible for a low Z material such as air. However, from satellite observations (O'Brien, 1962, for example), this does not seem as small as shown by laboratory experiments (Grün, 1957, Frank, 1959). Since laboratory data are limited to vertical (or normal) incidence only, it seems necessary to show the dependence of back-scattering on the incident angle, helpful in studying the so-called conjugation phenomena. Fig. 4 (a-b) shows angular dependence of the back-scattering coefficient for $E_0 =$ 20 and 2.5 Kev with respect to intensity (particle flux) and energy flux. The horizontal lines in each figure correspond to isotropic incidence.

3.5 Energy dependence of back-scattering

The results of Fig. 4 are replotted against energies in Fig. 5 (a, and b) for vertical incidence and isotropic incidence, respectively. It is well known that those coefficients decrease at high energies (Wu, 1960; Frank, 1959). Therefore, from the present results it can be concluded that the back-scattering of electrons has a maximum at an energy around 20 Kev, of the order of 7% for vertical incidence and more than 20% for isotropic incidence and that corresponding energy back-scattering is 4% and 14% for vertical and isotropic incidence, respectively.

It is interesting to see that the effect of straggling is reversed around 10 Kev for the isotropic incidence. At any rate, a decrease of back-scattering at low energies can be explained as follows: because of the spread in energy distribution after several collisions the amount of low energy electrons increases and these low energy electrons are unable to leave the air even though they are back scattered. On the other hand, a decrease of back-scattering at a high energy is simply due to the fact that the transformed distribution in the laboratory system is concentrated forward, even though scattering distributions in the center of mass system of colliding particles are regarded as isotropic.

3.6 Application for auroral electrons

Fig. 6 (a, b) shows the intensity and energy flux distribution of mono-energetic 20 Kev electrons in the atmosphere (CIRA, 1961) for vertical and isotropic distribution, respectively.

Fig. 7 (a, b) shows similar curves for 2.5 Kev electrons.

It is seen that the effect of straggling is negligible and even reversed below 5 Kev, whereas above 20 Kev the distribution of penetrating electrons due to straggling is significantly increased and nearly 1% exceed the range given by a continuous energy loss formula. Differentiating these curves with respect to altitude $\bar{Z}$, gives the vertical distribution of energy dissipation of auroral electrons. Fig. 8 shows one example for 20 Kev electrons. Here again the effect of straggling is significant. It should be noted that not only the most penetrating depth but also the height of maximum dissipation shifts to a lower altitude, i.e., to a deeper atmosphere.

Changes of angular distributions with altitude are shown in Fig. 9 (a, b) for mono-energetic 20 Kev electrons where relative intensities normalized to the initial intensity are plotted against the cosines of angles from normal directions. The change of angular distribution is similar for different energies as far as they are expressed with respect to x. It should be noted that angular distributions rapidly approach perfect diffusion with cosine square distribution, rather than Gaussian distribution, around half of the penetrating depth (Wu, 1960) for both cases of incidence distribution (vertical and isotropic). For a comparison cosine square curve is drawn in both cases. Fig. 10 (a, b) shows the plotting of a figure similar to Fig. 9 with the angle from the normal direction as a parameter. It should be noted that there is a maximum height (i.e., depth) in the intensity for oblique direction in the case of normal incidence, while intensity in the vertical direction decreases monotonically in both cases.

Finally, Fig. 11 shows the change of the energy spectrum of mono-energetic 20 Kev electrons with altitude. Full and dashed lines correspond to vertical and isotropic incidence, respectively. In the bottom, energies correspond to continuous energy loss, i.e.

$$E_m = E_0 - \cdot - \int_0^x \frac{dE}{dx'}, \, dx'.$$

It is interesting to note that the energies corresponding to the maximum intensities at each altitude (or depth) are considerably higher than E_m.

4. Conclusion

From the results of the present calculations we can draw the following conclusions.

(1) As seen from Fig. 1, 2, and 11, the values for the intensities and energy fluxes of electrons, based on conventionally used range-energy relations, are significantly underestimated.

(2) Because of the straggling effect, not only the depth of the tail of the penetrating electrons (Figs. 6 and 7), but also the depth of maximum intensity, shifts toward a deeper atmosphere, i.e., a lower altitude for a given energy of incident electrons.

(3) The back-scattering coefficient decreases rapidly below 10 Kev (Fig. 5). Since this coefficient also decreases at high energies, we can

conclude that back-scattering is largest around 20 Kev (between 10 and 25 Kev*) which is the order of 7%, and 20% for vertical and isotropic incidence, respectively for intensity, nearly half of these values for energy flux.

Table I

E_0 Kev	r_0 g cm^{-2}	Z_0 Km
20	$9.824 \cdot 10^{-4}$	93.24
10	$2.909 \cdot 10^{-4}$	100.18
5	$8.79 \cdot 10^{-5}$	107.13
2.5	$2.76 \cdot 10^{-5}$	118.02

*The value at 25 Kev is slightly less than that at 20 Kev.

REFERENCES

Berger, M. J.	1963	Methods in Computational Physics, V. I, pp. 135-215, Academic Press, New York
Berger, M. J. and Seltzer, S. M.	1964a	NASA Special Rept. SP-3008
Berger, M. J. and Seltzer, S. M.	1964b	Nat. Acad. Sci.-Nat. Res. Council, Publ. No. 1133 (Rept. No. 101)
Blunck, O. and Leisegang, S.	1950	Zeitschrift für Phys, 128, 500
Frank, H.	1959	Z. Natfasch 14A, 247
Goudsmit, S. and Saunderson, J. L.	1940	Phys. Rev. 57, 24
Grün, A. E.	1957	Z. Naturforsch 12A, 89
Kallman-Bijl, H., Boyd, R. L. F., Lagow, H., Poloskov, S. M. and Priester, W.	1961	Cospar International Reference Atmosphere (C.I.R.A), Interscience, New York
Landau, L.	1944	J. Phys. (Acad. Sci. U.S.S.R.) 8, 201
Maeda, K.	1962	NASA Tech. Rept. TR-R-141
Maeda, K.	1963a	J. Geophys. Res. 68, 185
Maeda, K.	1963b	Proc. International Sym. Strato. Mesopheric Circulation 36, 451
Maeda, K. and Singer, S. F.	1961	Arkiv Fysik 3, 531
Moliere, G.	1948	Zeits. f. Naturfors. 3A, 78
Mott, N. F.	1929	Proc. Roy. Soc. A124, 425
O'Brien, B. J.	1962	Z. Natfasch 14A, 247
Perkins, J. F.	1962	Phys. Rev. 126, 1781

Rees, M. H.   1963   Planet. Space Sci. $\underline{11}$, 1209

Rohrlich, F., and   1954   Phys. Rev. $\underline{93}$, 38
Carlson, B. C.

Rossi, B.   1952   High Energy Particles, p. 440,
                                       Prentice-Hall, New York

Spencer, L. V.   1959   Nat. Bur. Standards Monograph 1

Wu, C. S.   1960   Nuclear Spectroscopy Part A,
                                       pp. 15-30, Academic Press,
                                       New York

Figure 1—Relative intensities of penetrating the mono-energetic electrons in air $I(x)/I_0$ vs. depth of air x, where $x = r/r_0$ with r in g/cm^2 and r_0 is the practical range of electrons in g/cm^2, corresponding to the initial energy E_0 as shown in Table I

(a) $E_0 = 20$ Kev, (b) $E_0 = 2.5$ Kev

The full and dashed lines stand for the calculations with straggling and without straggling, respectively. Thick lines and thin lines correspond to isotropic incidence and vertical incidence respectively.

Figure 2—Relative energy fluxes of mono-energetic electrons $E(x)/E_0$ vs. the depth of air x, corresponding to the different initial energies shown in Figure 1. All notations are the same as in Figure 1.

Figure 3—Relative energy dissipation curves of mono-energetic electrons $(\Delta E/E_0)/(\Delta r/r_0)$ vs. depth of air x, corresponding to different initial energies shown in Figures 1 and 2. All notations are the same as those used in Figures 1 and 2.

Figure 4—Back-scattering vs. incident (or incident pitch) angle of a mono-energetic electron beam. Full and dashed lines stand for the calculations with straggling and without straggling, respectively. Thick lines and thin lines correspond to particle flux (intensity) and energy flux, respectively.

Figure 5—Back-scattering coefficients vs. of incident energy. The two figures (a and b) correspond to two cases for incident angles of mono-energetic electrons, i.e., (a) vertical incidence, (b) isotropic incidence.

Figure 6—Relative intensity (particle flux) and relative energy flux of electrons with an initial energy of 20 Kev vs. altitude (in km) in the CIRA (1961) model atmosphere. The height indicated by Z_0 corresponds to the maximum penetration depth corresponding to practical range for the initial energy of electron E_0 = 20 Kev. Full and dashed lines correspond to calculations with straggling and without straggling, while thick lines and thin lines stand for intensity and energy flux, respectively, (a) vertical incidence, (b) isotropic incidence.

Figure 7—Intensity and energy flux distribution of mono-energetic 2.5 Kev electrons. All notations are the same as in Figure 6.

Figure 8—Energy dissipation curves for electrons with initial energy E_0 = 20 Kev in the atmosphere, CIRA (1961) model.

Figure 9 (a, b)—Angular distribution (relative intensity/steradian) electrons with initial energy E_0 = 20 Kev. The symbol x indicates nondimensional atmospheric depth r/r_0 where r_0 = 9.824 × 10^{-4} g/cm^2. (A) vertical incidence, (b) isotropic incidence.

Figure 10 (a, b)—Plots similar to Figure 9 for relative intensity against nondimensional depth x for different zenith (or pitch) angles θ. (a) vertical incidence, (b) isotropic incidence.

Figure 11—Differential energy spectrum of initially mono-energetic electrons, E_0 = 20 Kev, in the atmosphere. Altitudes shown in parenthesis are the altitudes in CIRA (1961) atmosphere, corresponding to non-dimensional depth x.

E_m shown in the bottom corresponds to the energy given by the conventional energy-range relation i.e.,

$$E_m = E_0 - \int_0^x \frac{dE}{dx'} dx'$$

where dE/dx'is given by the Bethe formula as a function of energy.

Full lines and dashed lines stand for the vertical and isotropic distributions of incident electrons, respectively.

FIGURE 1

E_0 = 20 Kev

ISOTROPIC

WITH STRAGGLING

NO STRAGGLING

VERTICAL

(a)

$E(x)/E_0$

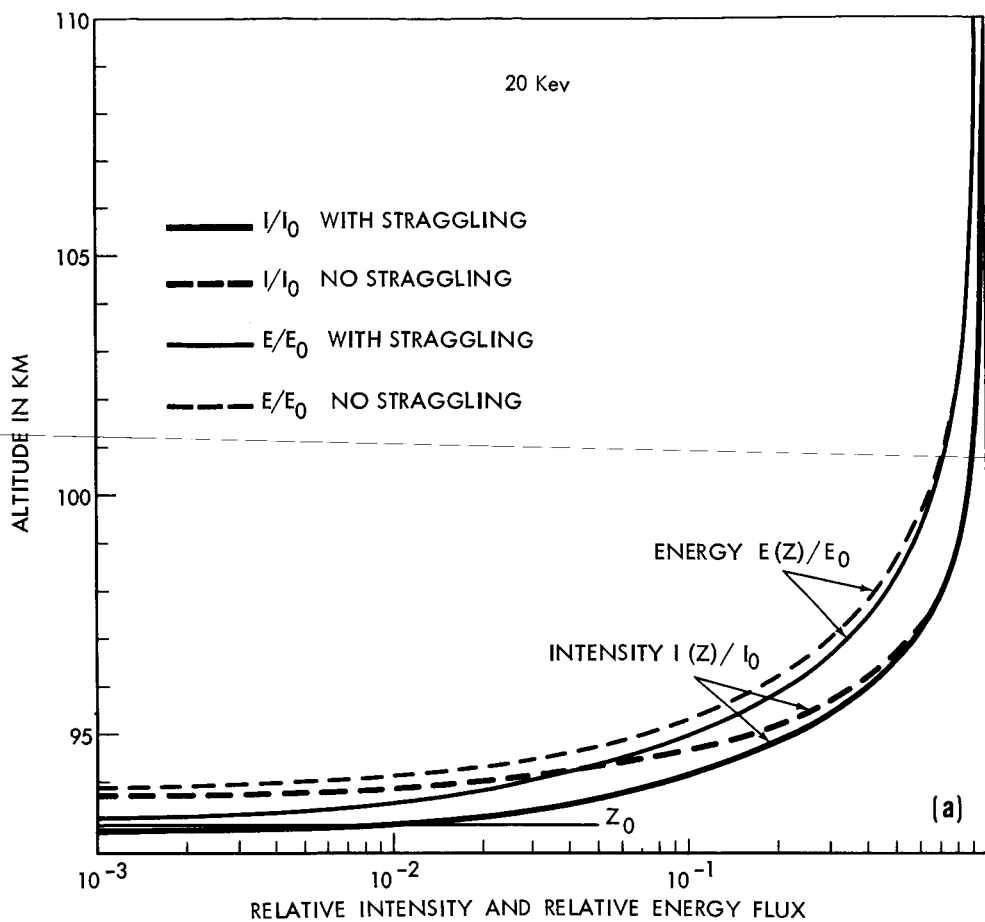E_0 = 2.5 Kev

ISOTROPIC

VERTICAL

WITH STRAGGLING

NO STRAGGLING

(b)

$E(x)/E_0$
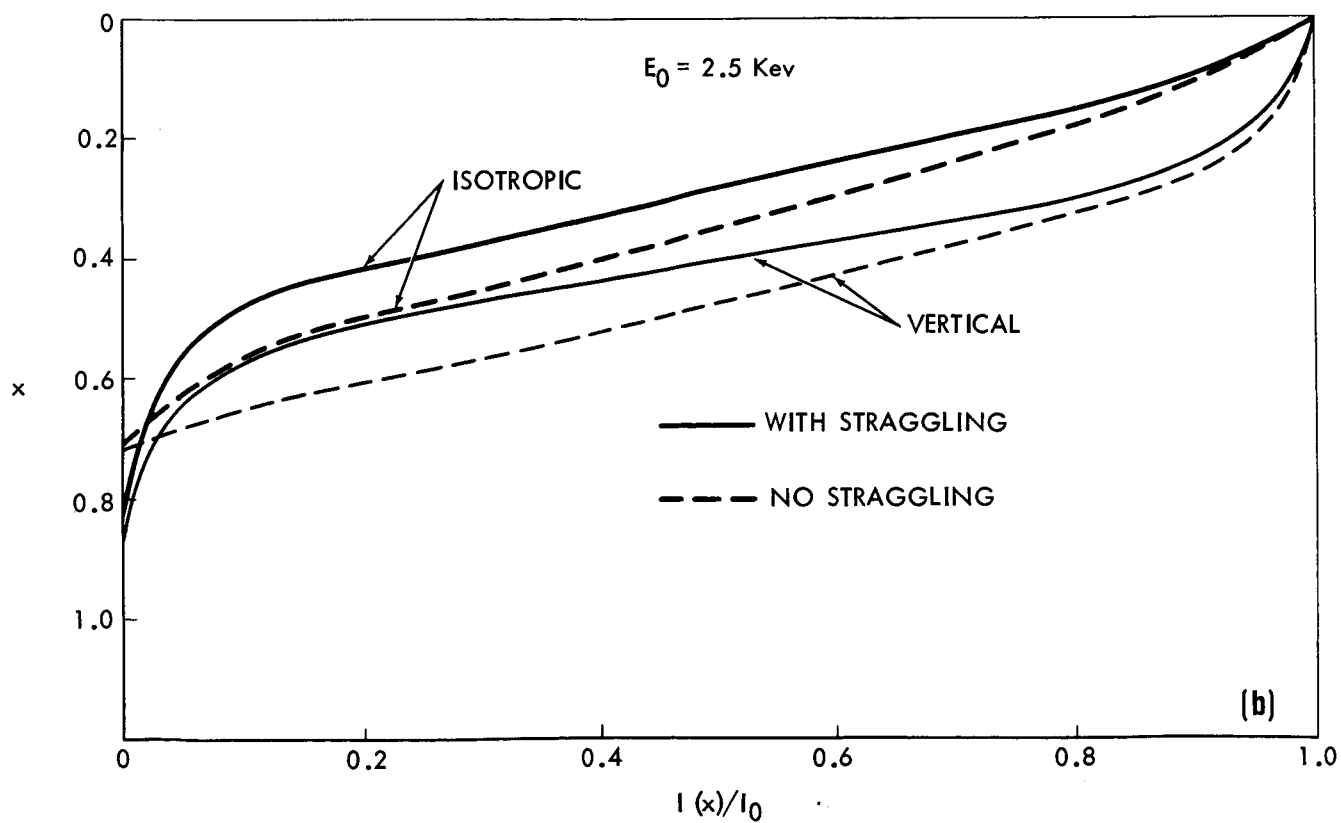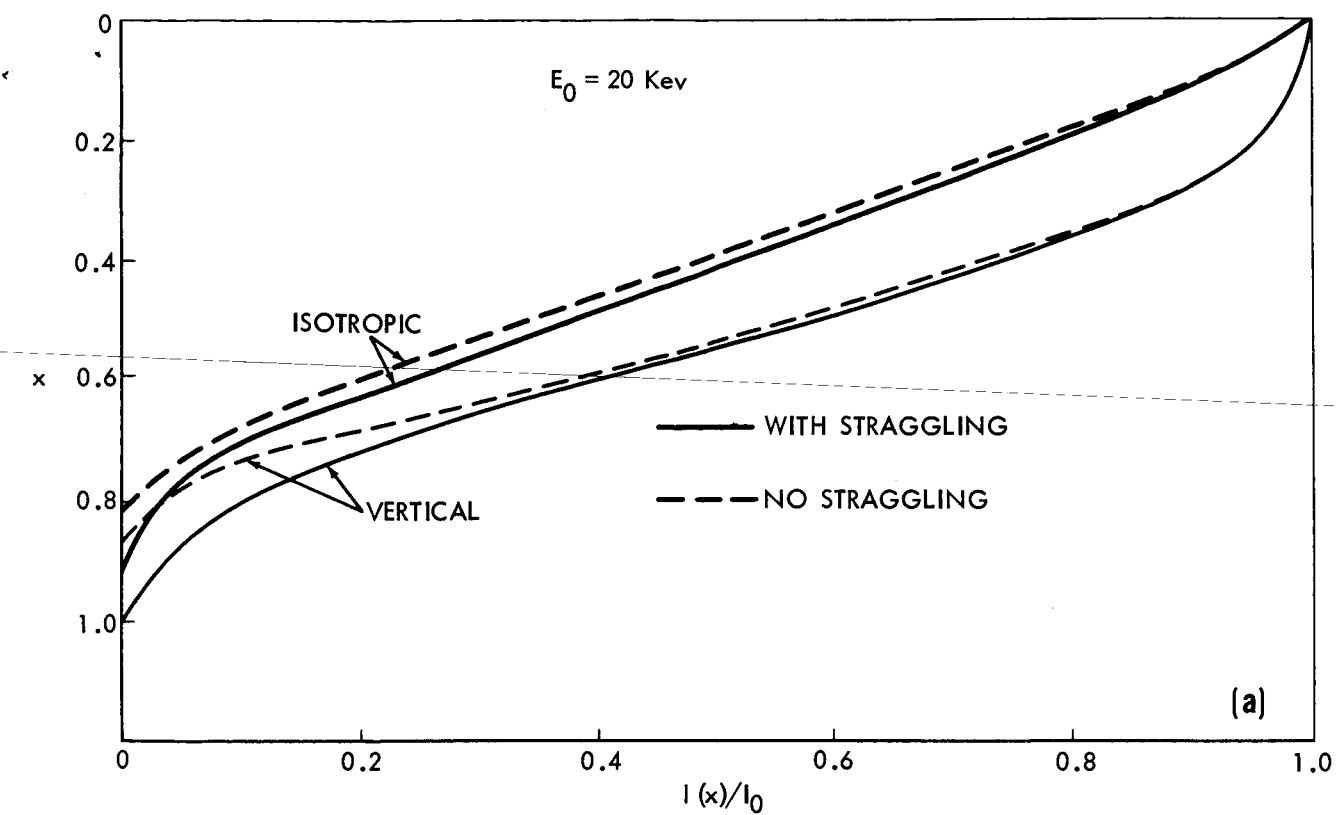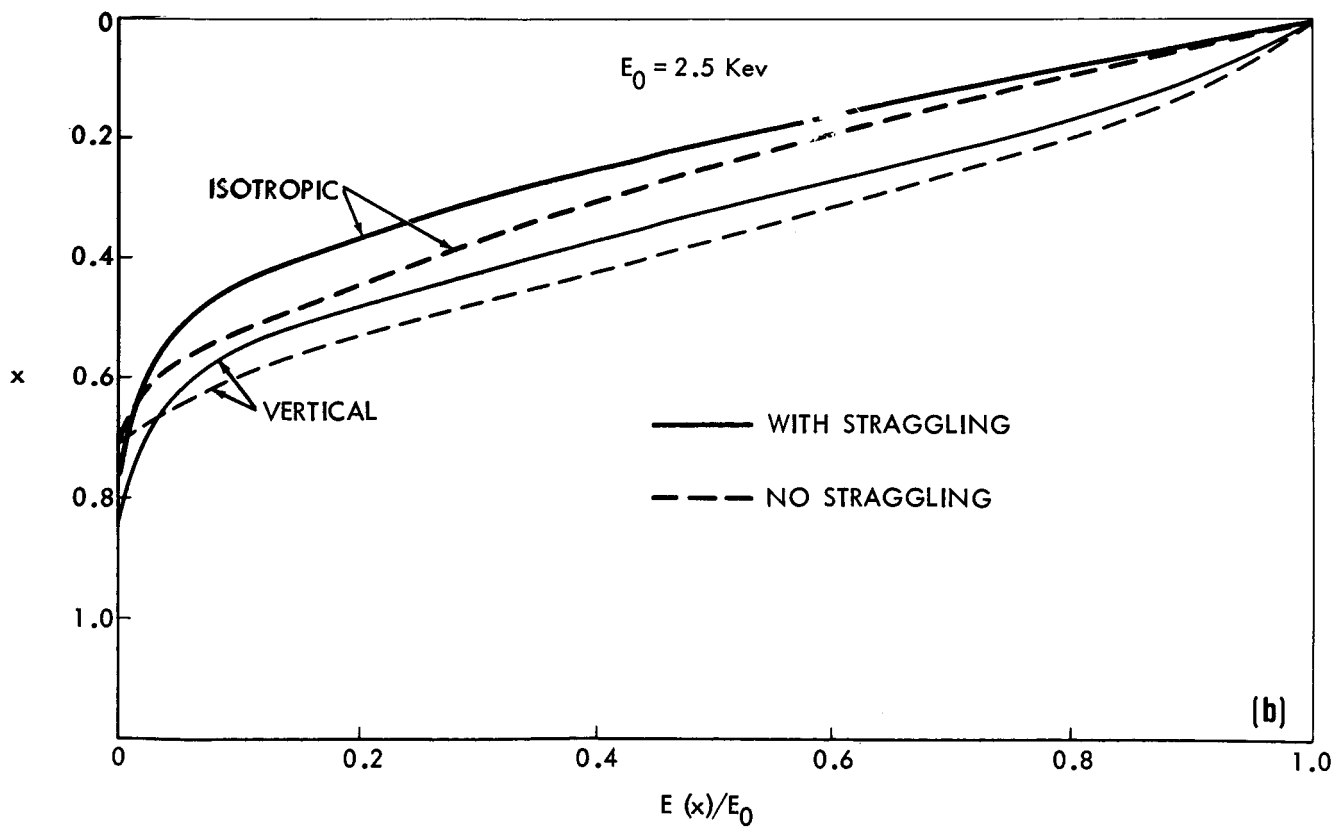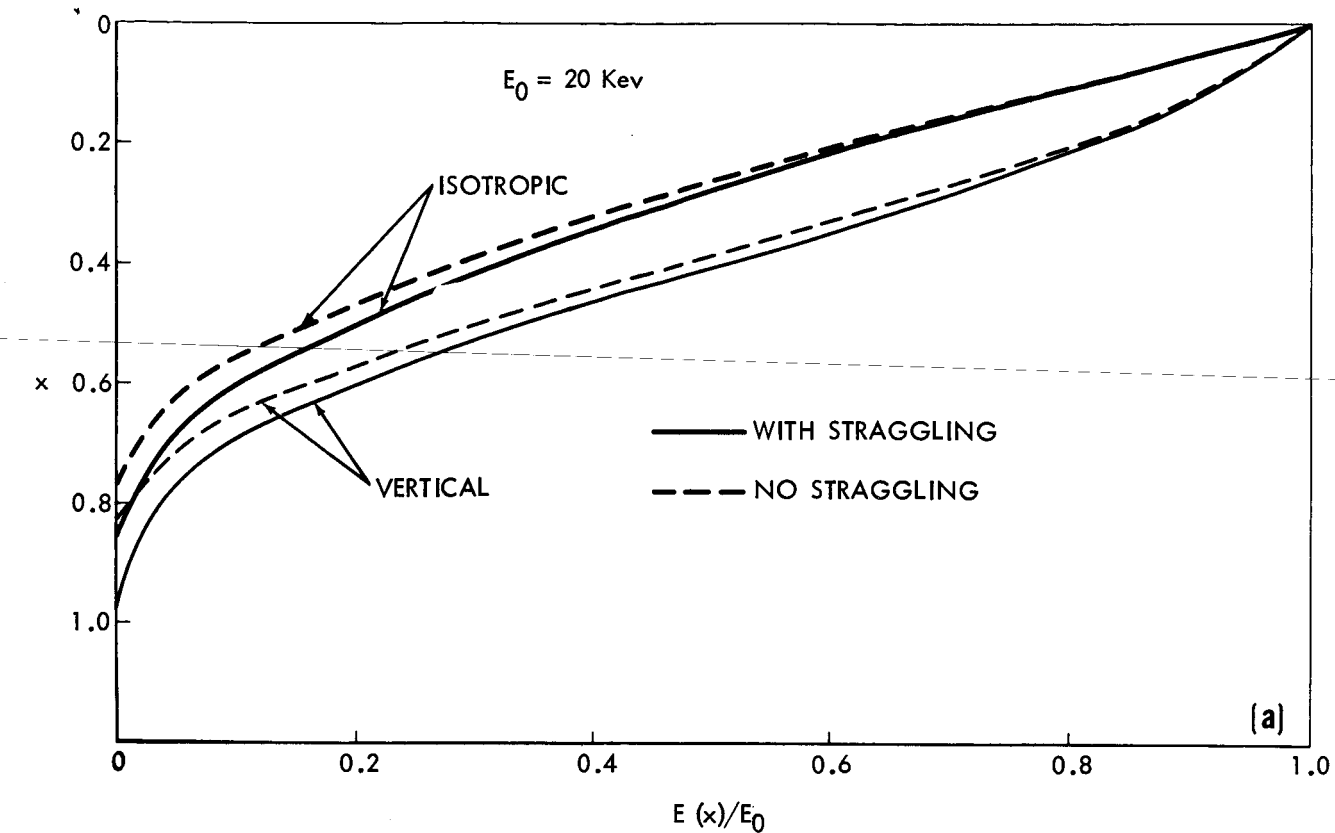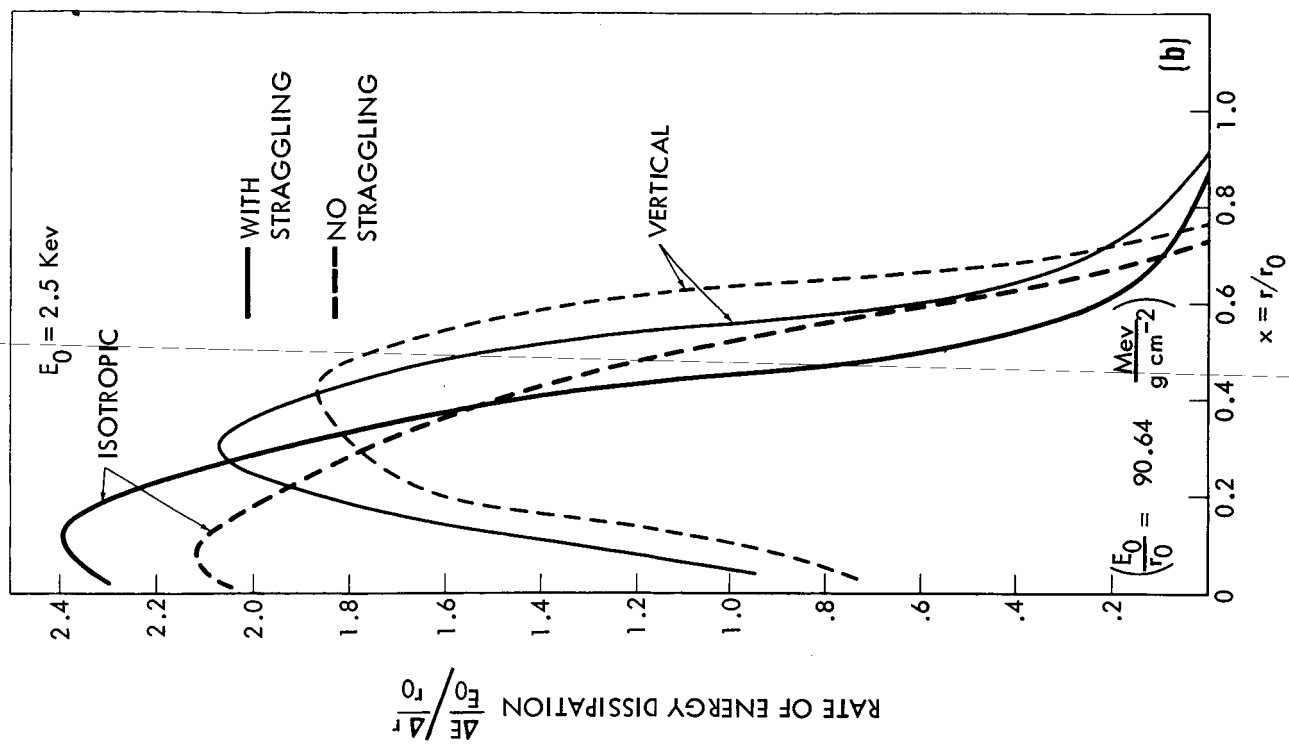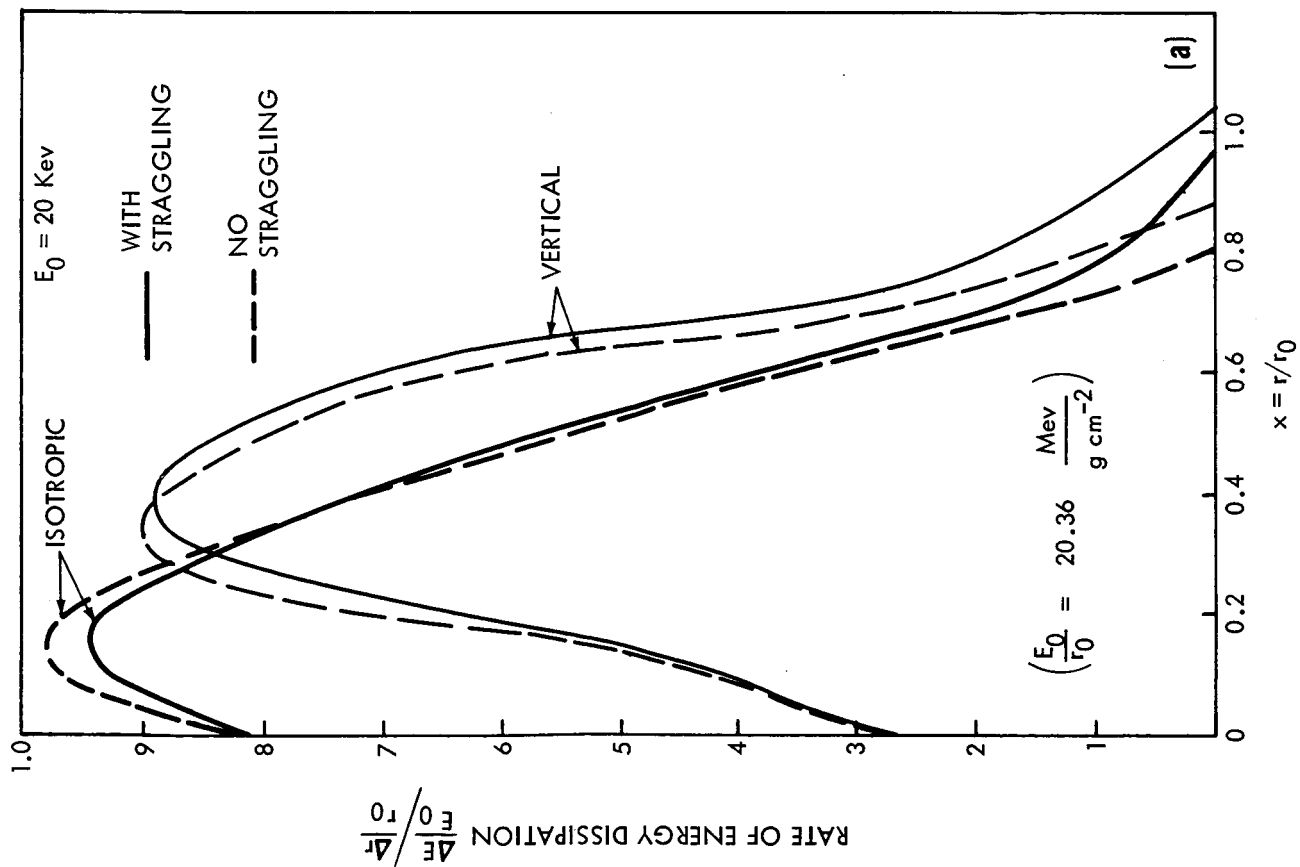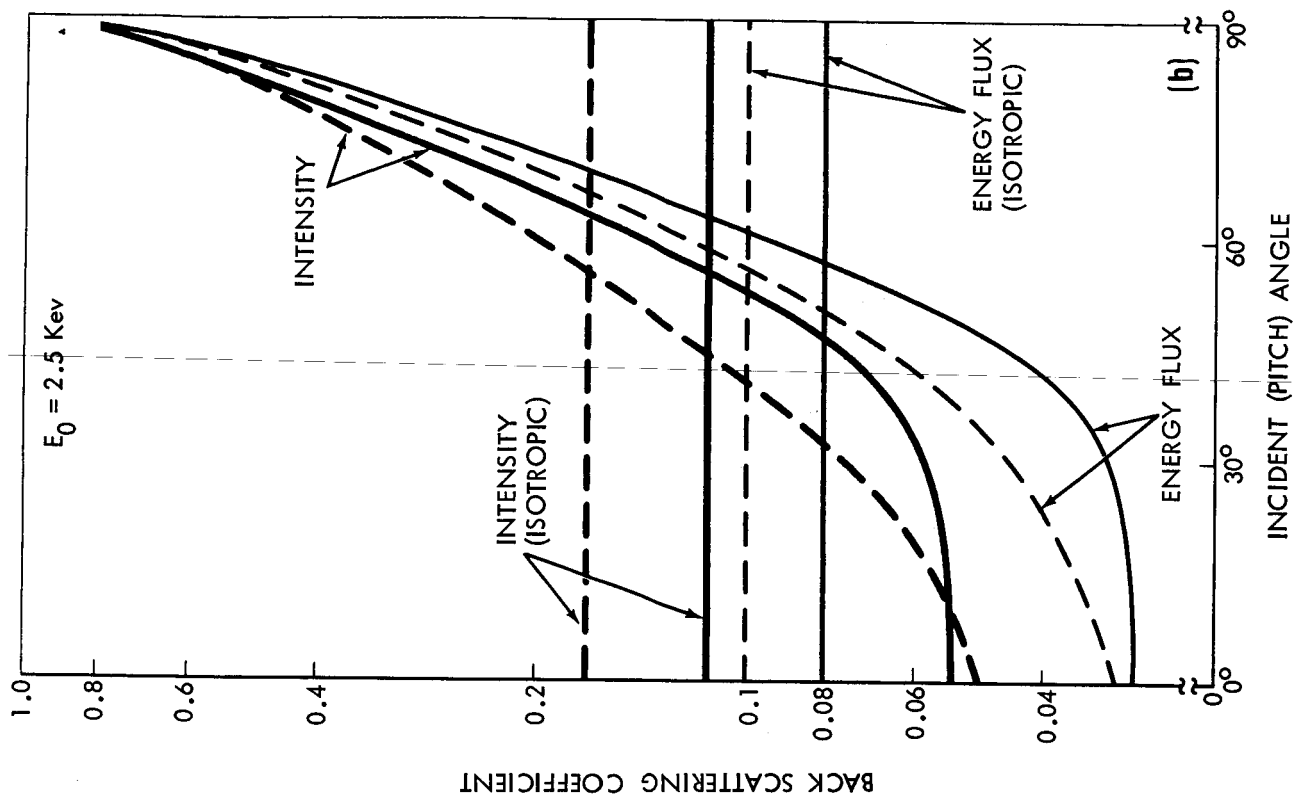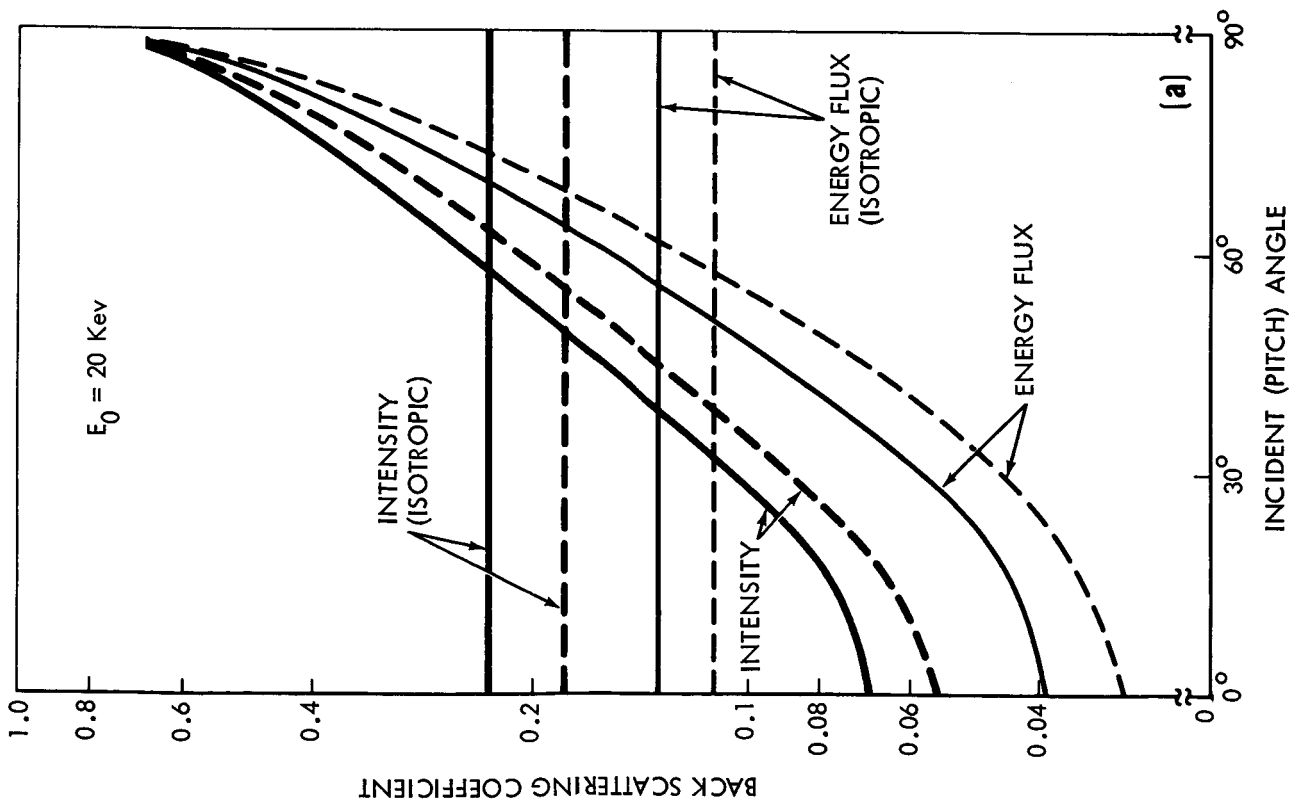
FIGURE 2
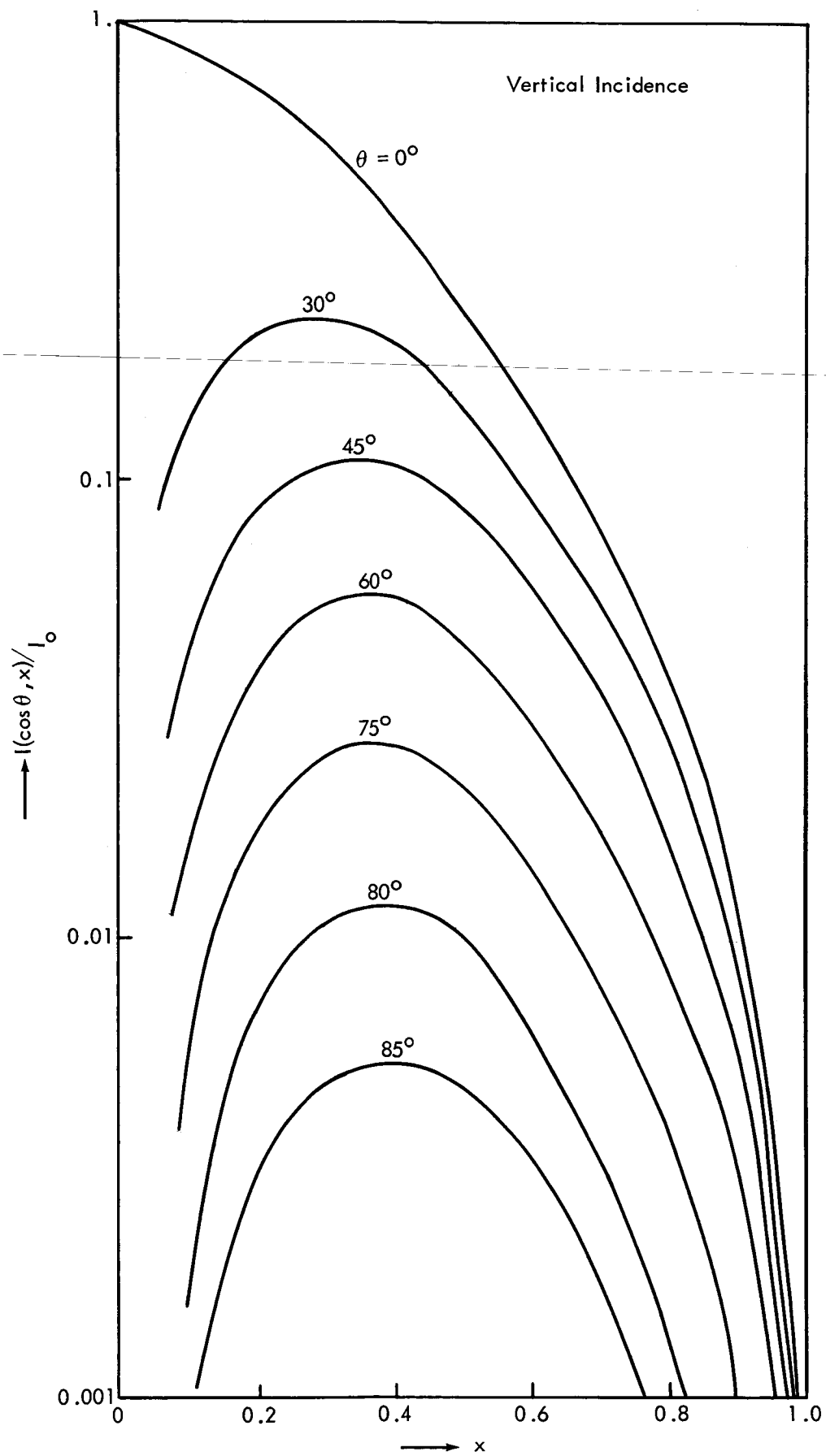
FIGURE 3

FIGURE 4
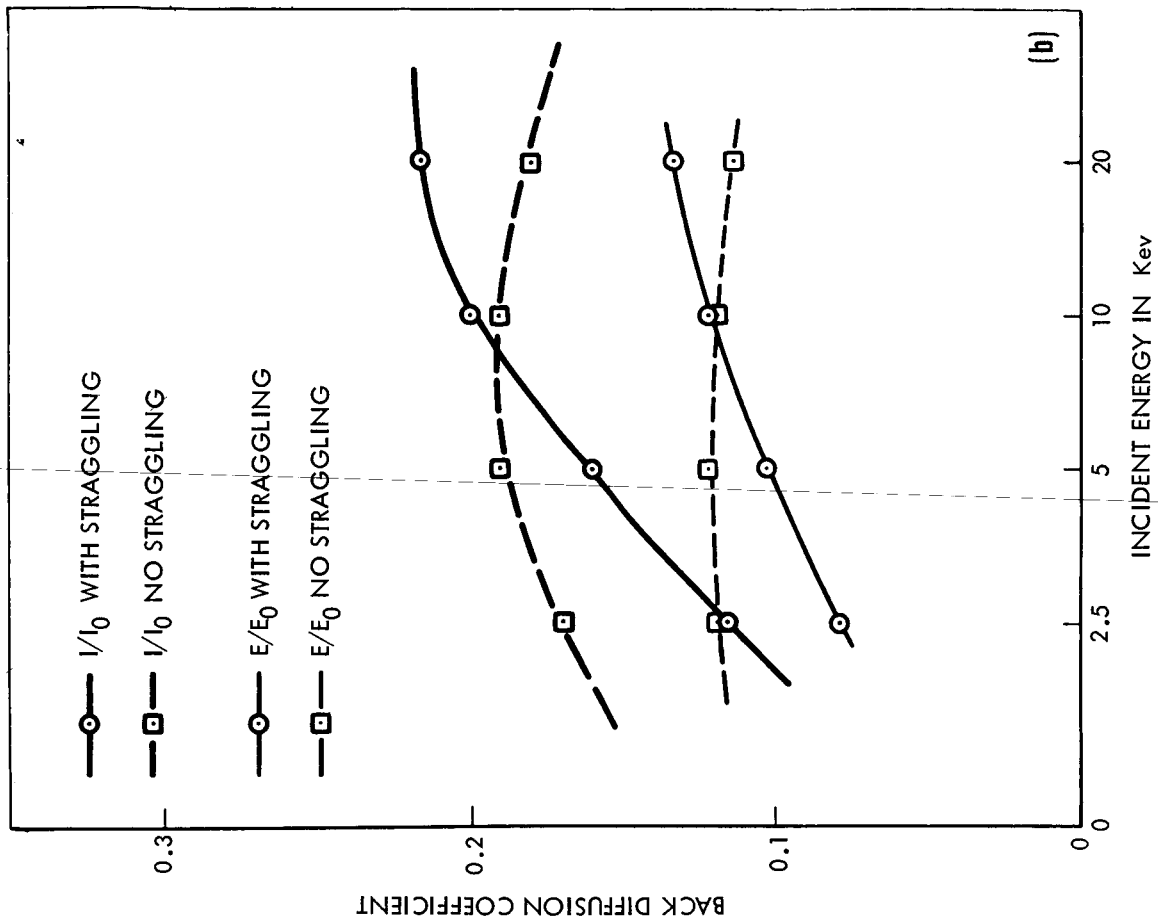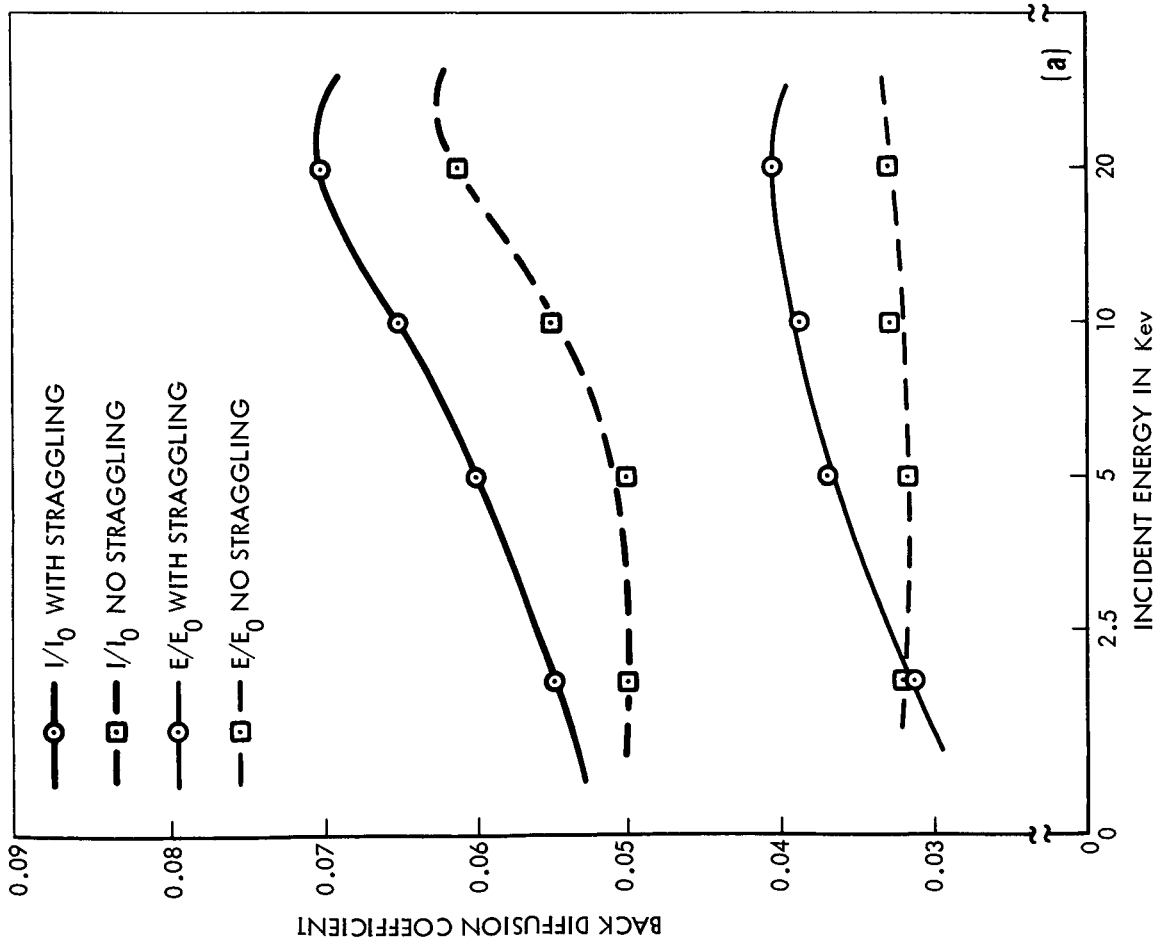
FIGURE 5
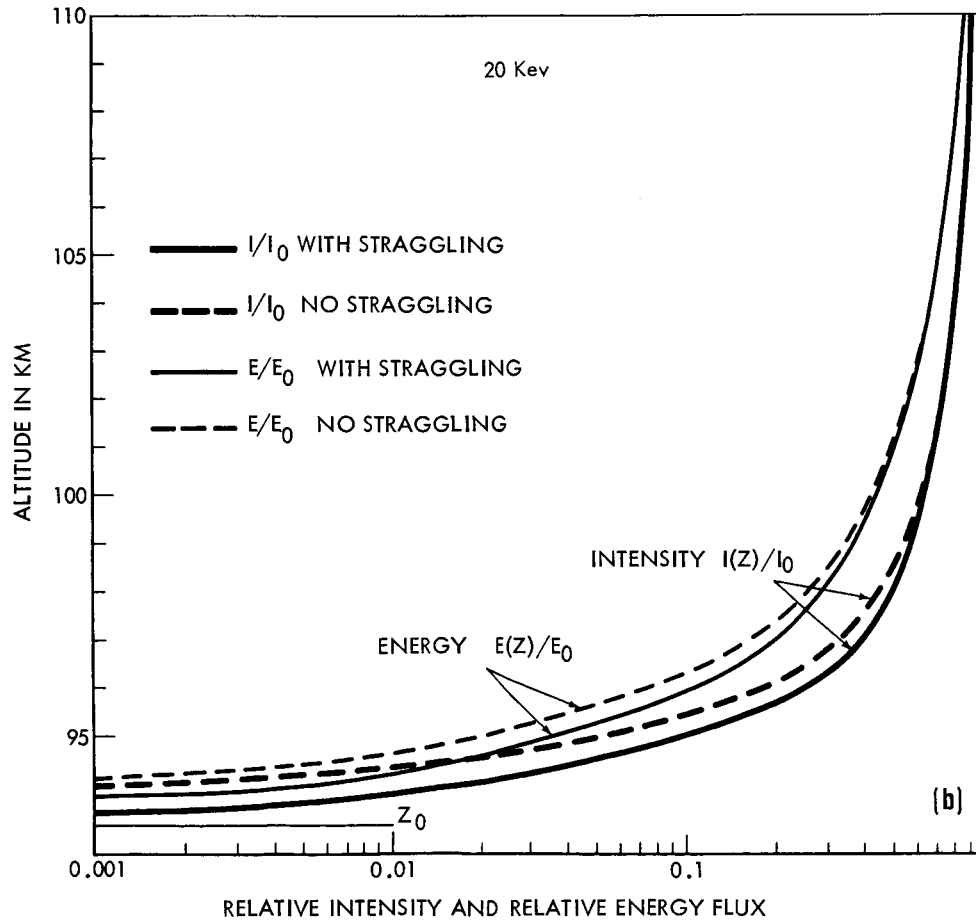
FIGURE 6
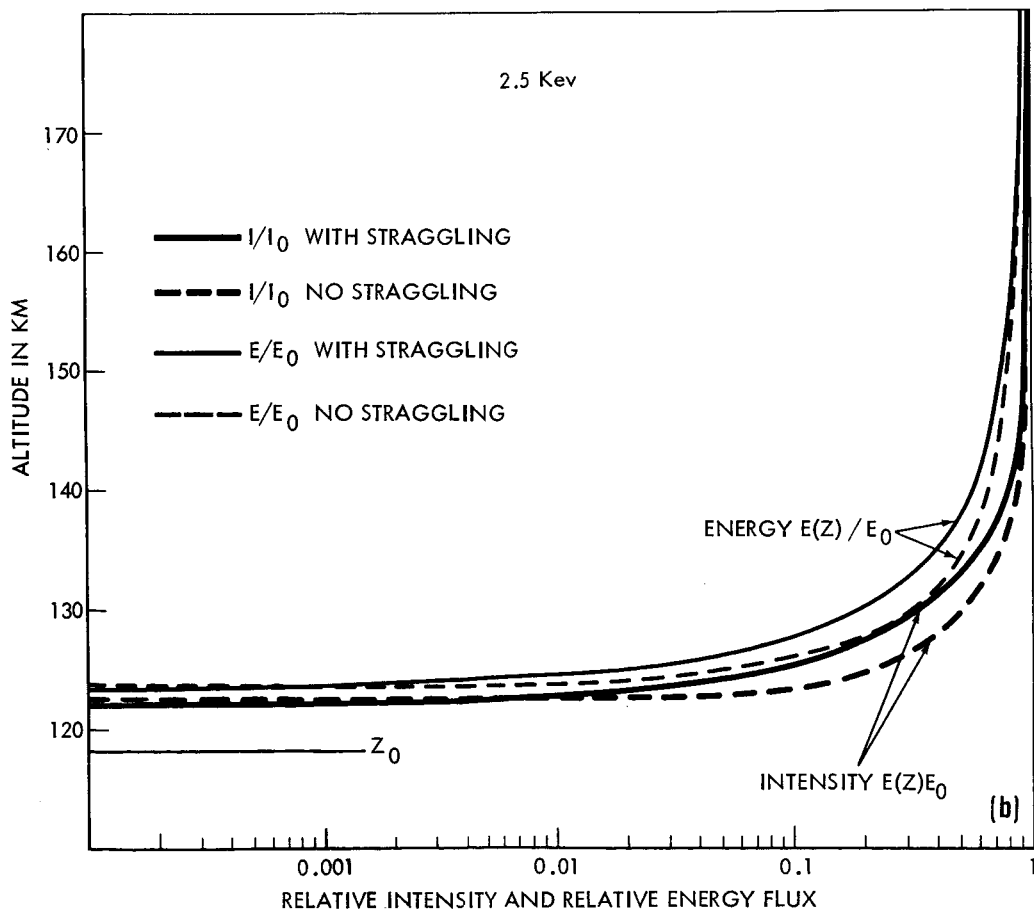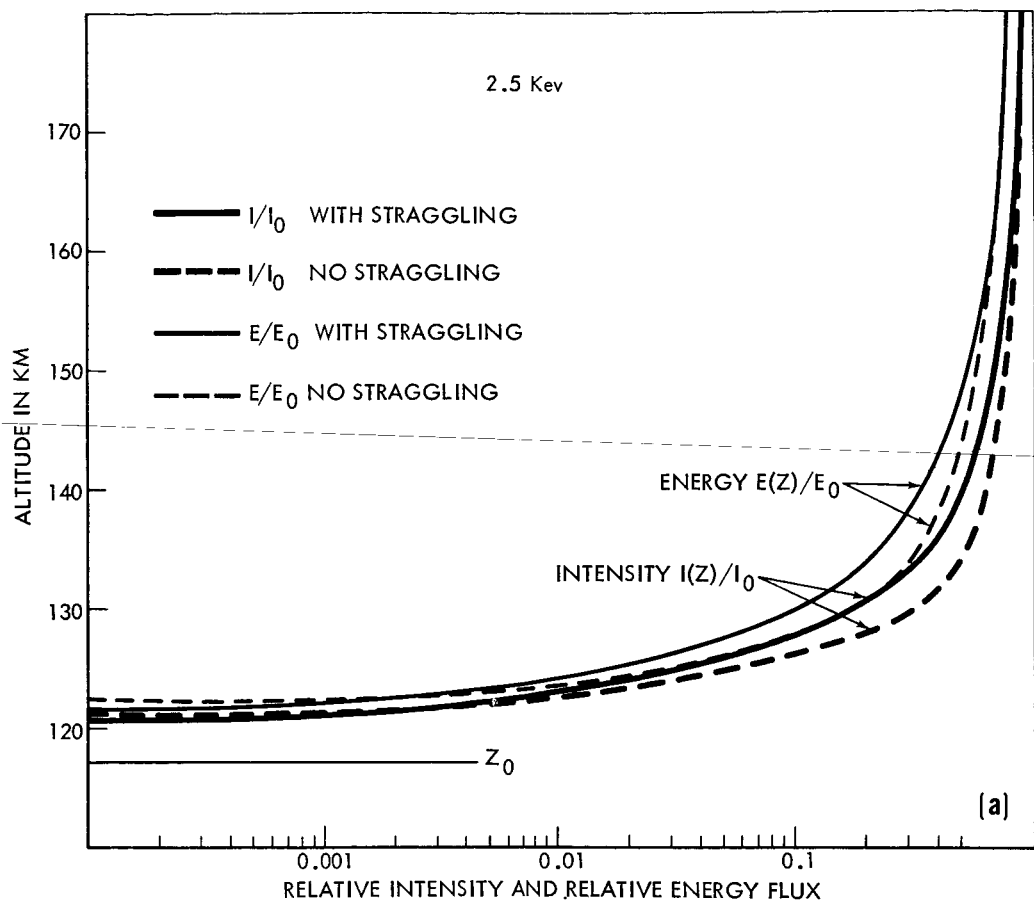
FIGURE 7
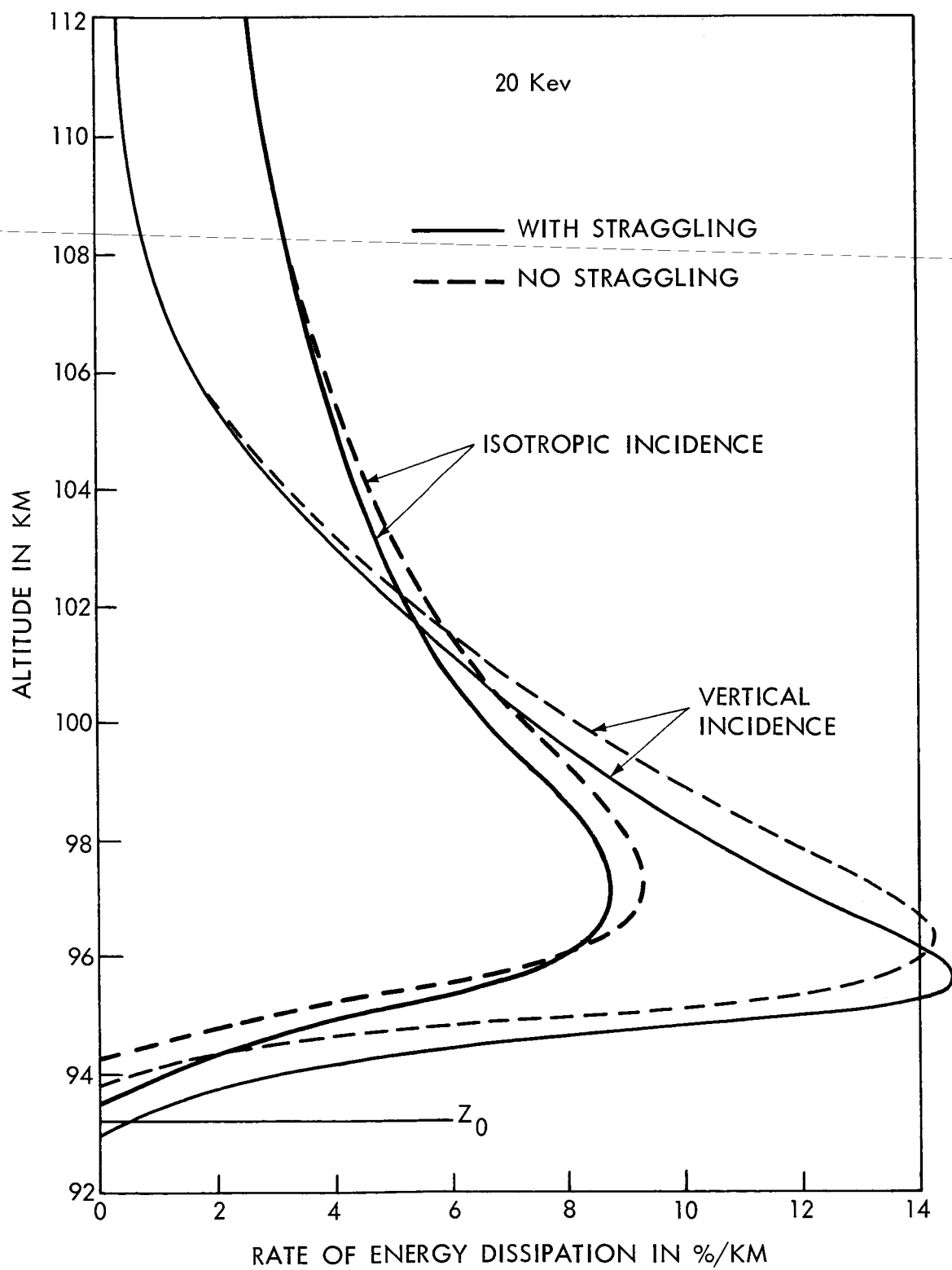
FIGURE 8
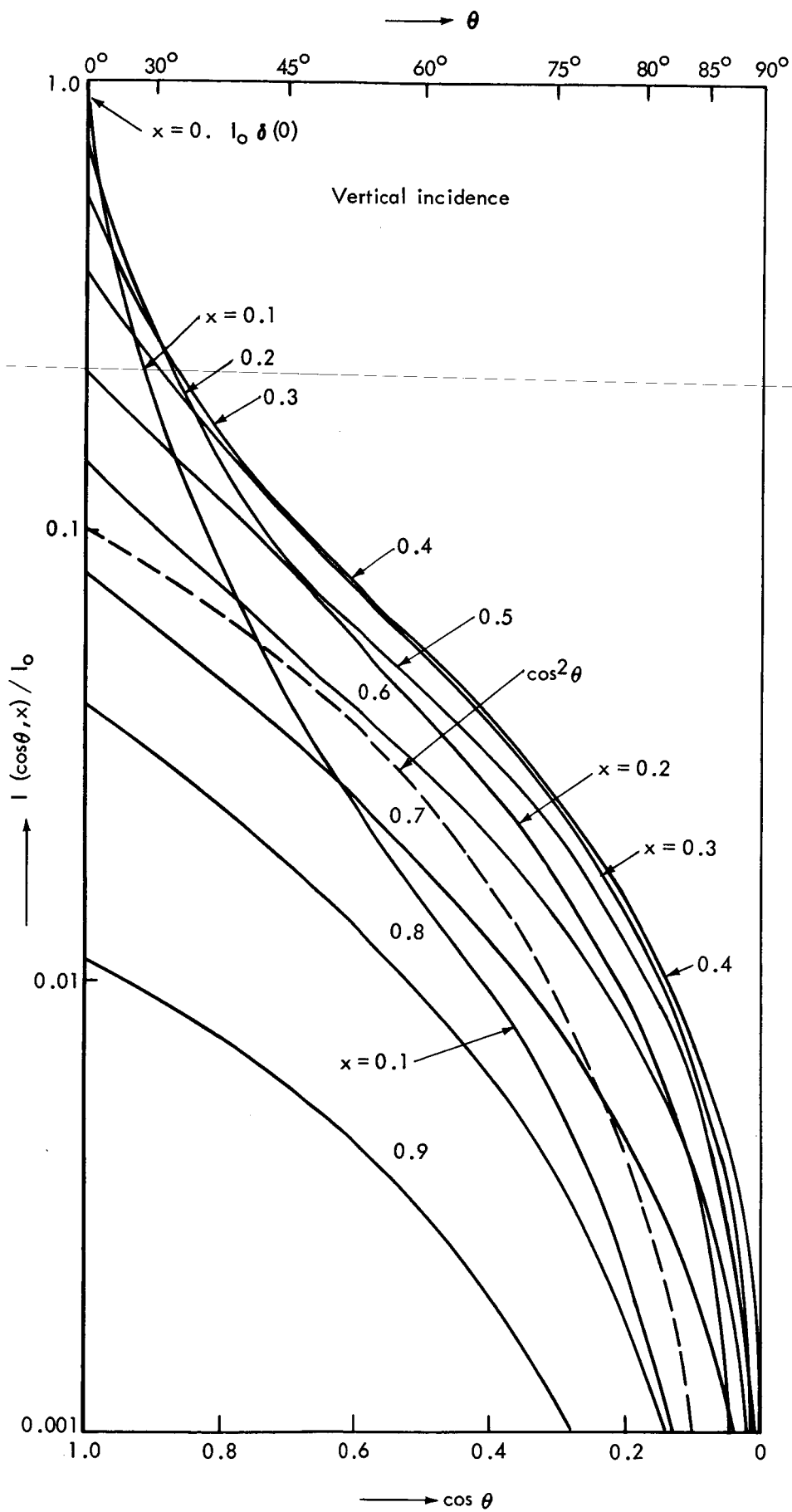
FIGURE 9 (a)
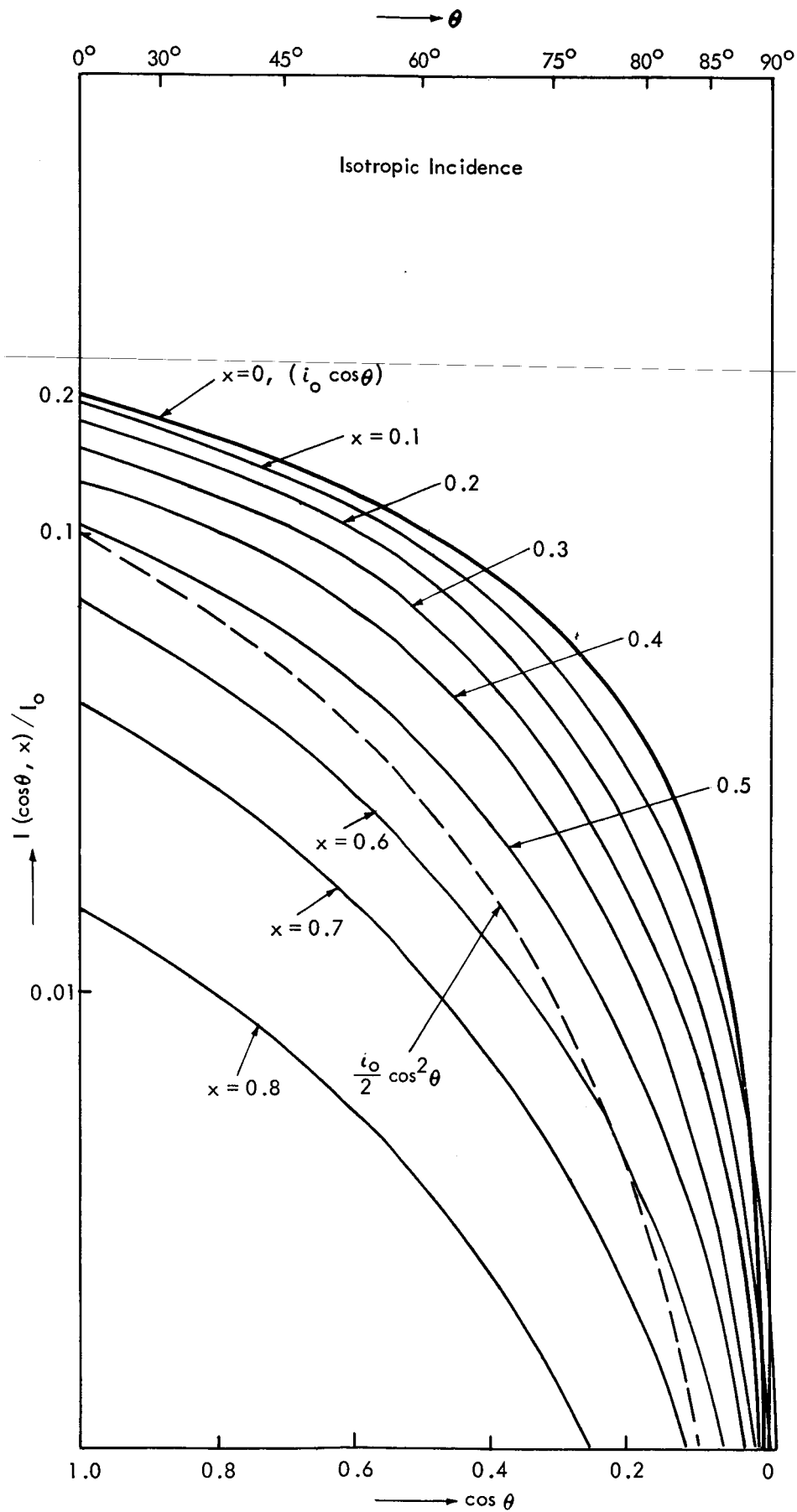
FIGURE 9 (b)

FIGURE 10 (a)

FIGURE 10 (b)

FIGURE 11